Journal of Materials Chemistry C

Accepted Manuscript

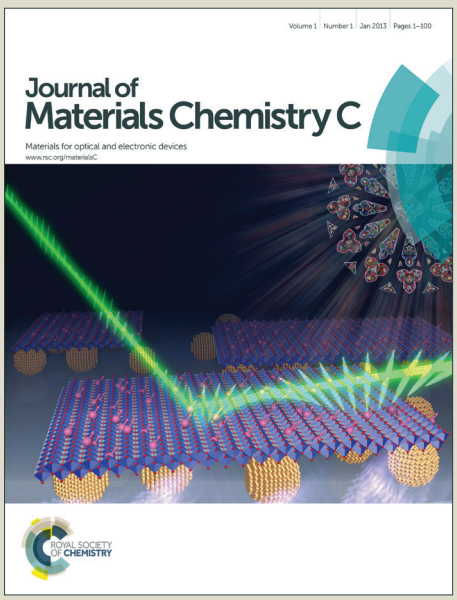

ROYAL SOCIETY OF CHEMISTRY

www.rsc.org/materialsC

Preparation of water-dispersible graphene using *N*-methylmorpholine *N*-oxide monohydrate and its application for preparing nanocomposites with PEDOT

Dong-Hun Kim[1], Loon-Seng Tan[2], and Soo-Young Park[1,*]

[1]Major in Polymer Science and Engineering, School of Applied Chemical Engineering, Kyungpook National University, #1370 Sangyuk-dong, Buk-gu, Daegu 702-701, Republic of Korea

[2]Soft Matter Materials Branch (RXAS), Materials & Manufacturing Directorate, Air Force Research Laboratory, Wright-Patterson AFB, OH 45433, USA

* Corresponding author (psy@knu.ac.kr)

Abstract: Solid-state powders of water-dispersible graphene (GPN) were prepared by treatment of methylmorpholine *N*-oxide monohydrate ($NMMO_m$). Re-dispersion of GPN in water by simple sonication was successfully demonstrated with a highly concentrated aqueous GPN solution (0.284 mg/mL) after centrifugation at 9000 rpm for 10 min. The produced GPN had the graphitic structure without defects, and its electrical conductivity was 94.7 S/cm, as measured from a filtered GPN film. The spin-coated thin film from the aqueous GPN solution exhibited a single-layered structure, which was examined using scanning electron microscopy, atomic force microscopy, and scanning transmission electron microscopy (with selective area electron diffraction). The GPN was also dispersible in polar solvents such as dimethyl sulfoxide, dimethylformamide, ethanol, and tetrahydrofuran. The origin of good dispersity of GPN in polar solvents, including water, was discussed with reference to the high polar nature of NMMO. A nanocomposite system with a water-soluble poly(3,4-ethylenedioxythiophene):poly(styrenesulfonate) (PEDOT:PSS) was prepared on a glass substrate. A fourfold improvement in the electrical conductivity of PEDOT:PSS without deterioration of the transmittance was achieved by adding 1 wt% GPN.

Key words: Graphene, water-dispersible, *N*-methyl morpholine *N*-oxide (NMMO), nanocomposite, poly(3,4-ethylenedioxythiophene).

Introduction

Graphene combines unique electronic properties and surprising quantum effects with outstanding thermal and mechanical properties.[1-4] Several methods to prepare graphene, such as mechanical cleavage of highly ordered pyrolytic graphite (the "scotch tape" method),[5] chemical vapor deposition on metals,[6] epitaxial growth on SiC or metal substrates,[7,8] exfoliation from expanded graphite,[9,10] and reduction from graphene oxide (GO),[11-13] have been developed. One of these methods, the reduction of GO requires the oxidation of graphite powders to make the precursor of the reduced GO (rGO).[12,14] Although the oxidation processes developed can produce relatively large amounts of water-soluble GO compared with the other methods, the resulting GO also exhibits poor electrical and thermal properties due to the presence of many defects, such as wrinkling, crumpling, and atomic vacancies.[15-17] Thus, many promising macroscopic applications of graphene require the development of novel routes for producing graphene by effective and direct graphite exfoliation without the need for the oxidation step.

Coleman et al. developed the liquid-phase exfoliation of graphite to transform graphite into graphene through the sonication of graphite powder in well-selected liquids and aqueous surfactant solutions.[18,19] The selection rationale was based on the results of previous theoretical and experimental studies concerning the dispersion of carbon nanotubes in solvents.[20] The mechanism underlying the liquid-phase exfoliation process is driven thermodynamically in terms of the enthalpy of mixing for the dissolution of polymers in special liquids as well as the charge-transfer type specific donor-acceptor interactions between the carbon layers of graphite and the solvent molecules.[18,21] From the thermodynamic perspective for mixing, organic solvents with surface tensions (or energies) similar to that of graphene (40 to 50 mJ/m^2) are likely to be an effective dissolution media.[18,21] Benzyl benzoate, 1-methyl-2-pyrrolidinone (NMP), γ-butyrolactone (GBL), *N,N*-

dimethylacetamide (DMAc), *N*-vinyl-2-pyrrolidone (NVP), and *N,N*-dimethylformamide (DMF), which have surface energies matching that of graphene, could be classified as good exfoliating reagents, whereas others, such as ethanol, acetone, and water, which have surface energies that are significantly lower than that of graphene, are poor media for graphite exfoliation.[18,19,22] From the donor-acceptor interaction perspective, a few aromatic and non-aromatic solvents with either strong electron-withdrawing or electron-donating functional groups could be used as media for exfoliating and stabilizing graphene via the charge transfer between the solvent molecules and graphite layers.[9,22-25] Such specific interactions would result in carbon atoms with localized charges in graphite not being able to participate in the π-bonding network,[26] and significantly weaken the van der Waals attraction between the graphite inter-layers. The efficient exfoliation of graphite in highly ionic media such as ionic liquids[27,28] and chlorosulfonic acid (through protonation),[4] are likely driven by the charge transfer mechanism as well.

The solvents mentioned as effective dissolution media tend to be nonvolatile[29] because solvents with surface tensions of ~ 40 mJ/m^2 (the Hildebrand solubility parameter approaches 23 MPa$^{1/2}$)[18,20,26] have a high boiling point, which can make them difficult to be removed when processing graphene into films or composites.[18] In particular, it is virtually impossible to deposit individual flakes from solvent-exfoliated graphene, as aggregation tends to occur during the slow solvent evaporation.[18] Although graphene dispersions in high-boiling-point solvents have been transferred into low-boiling point-solvents via solvent exchange,[22] it would be preferable to develop a method that allows the direct exfoliation of graphite to provide stable dispersions of graphene in low-boiling-point solvents. This method would greatly simplify graphene exfoliation and significantly expand the number of applications of liquid-exfoliated graphene. Graphene in low-boiling-point solvents, such as chloroform and isopropanol, was demonstrated to be exfoliated at relatively high

concentrations with a thickness of less than 10 layers (≤ 5 layers for isopropanol).[30] Homogeneous graphene dispersion was also achieved by the removal of aggregates through sonication of graphite in 1-propanol followed by centrifugation.[31] However, the concentration of the dispersion was still lower than that from other high-boiling-point solvents; it was possible to achieve concentrations of up to 0.5 mg/mL, which is just less than half of that achieved with high-boiling-point solvents such as NMP.[30]

Among low-boiling-point solvents, water would be the best choice as a medium for graphite exfoliation because it is cheap, easily available, and the most environmentally friendly solvent. However, the direct dispersion of hydrophobic graphite or graphene sheets in water without the assistance of dispersing agents has generally been considered an insurmountable challenge. The use of surfactants or hydrophilic organic molecules as dispersing agents is essential for dispersing the graphitic species in water.[9,19,32-36] Water-dispersible graphene can be easily applied in inkjet printing, spray- or spin-coating on various substrates and can be used as conductive binders with water-soluble polymers. The direct dispersion of graphene in water is based on the interactions between the dispersing agent and graphene through van der Waals forces, π–π and/or donor/acceptor interactions, and the electrostatic repulsions between the interacted dispersing agents. The dispersing agents can be small molecules or polymers with water-dispersible functional groups such as sodium dodecylbenzenesulfonate (SDBS),[19] sodium cholate (SC),[34] pluronic P-123,[35] 7,7,8,8-tetracyanoquinodimethane (TCNQ),[9] pyrenebutyric acid,[37] other pyrene (Py) derivatives including1-pyrene-methylamine (Py-NH_2) and 1,3,6,8-pyrenetetrasulfonicacid (Py-SO_3),[38] tryptophan,[39] rose bengal (RB),[40] polyvinylpyrrodine,[41] poly-L-lysine,[42] 6-amino-4-hydroxy-2-naphthalenesulfonic acid, and sulfonated polyaniline.[43] Recently, Li and co-workers reported that chemically converted graphene sheets could readily form stable aqueous colloids through electronic stabilization in the presence of ammonia.[44] However, the use of

these dispersing agents for preparing graphene can be a demerit because they can act as impurities in further applications. Thus, methods for preparing water-dispersible graphene without dispersing agents are highly desirable.

N-methylmorpholine *N*-oxide (NMMO) monohydrate ($NMMO_m$) has a water content between 13.3 and ~17 wt% and a melting point of 76 °C. Its liquid form at ~ 80 °C has been used as an organic solvent that is able to dissolve natural polymers in the industry of man-made regenerated cellulose fibers using the so-called "Lyocell" process.[45-48] The chemical structure of NMMO (as shown in Figure 1) has a high electron density on the oxygen, which is able to disrupt the hydrogen bonding in cellulose, causing a decrease in its crystallinity. The highly polar N–O bond (dipole moment of 4.38 mD) in NMMO allows NMMO to become extremely soluble in water by forming hydrogen bonds with water.[49] The N-O bond in NMMO can be readily broken and releases a relatively large energy of 222 kJ/mol upon cleavage. NMMO is a strong oxidant, thermally labile, and sensitive toward all types of catalysts that induce N-O bond cleavage. NMMO is a weak basic compound ($pK_B = 9.25$); the negatively charged exo oxygen acts as the proton acceptor. Importantly for this research, the surface tension of $NMMO_m$ is 44 mJ/m^2 at 80 °C,[50] which is well matched with that of the nanotube/graphite (40–50 mJ/m^2).[51-54] Thus, these close values between them lead to a complete miscible state such that the energy cost for exfoliation should be small compared with that for other solvents. One of the merits in using $NMMO_m$ is to store the as-exfoliated graphene for long time as graphene in $NMMO_m$ solids offers a solution to the challenge of large-scale graphene storage. Figure supplementary information (SI) 1 show a solidified graphene mixture with $NMMO_m$ at room temperature after one month later. This mixture could be used at any time for making GPN through heating, dilution with water, and filtration. Moreover, NMMO is non-toxic, inexpensive, and recyclable for industrial applications.

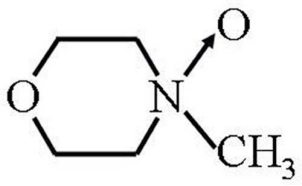

Figure 1. Chemical structure of NMMO.

In this work, $NMMO_m$ was employed as an exfoliating agent of graphite. Its close surface tension to graphite, the highly polar nature of the N-O bond, and the proton-acceptor property make it an ideal candidate. More importantly, the obtained graphene (GPN) could be dispersible in water at a high concentration, which opens the path toward new applications in inkjet printing, spray or spin-coating on various substrates for an optovoltaic cell, organic light-emitting diodes, and touch screen panels. To demonstrate the application of the prepared water-soluble graphene in a nanocomposite system, the water-soluble poly(3,4-ethylenedioxythiophene): poly(styrenesulfonate) (PEDOT:PSS) was hybridized with GPN. The PEDOT:PSS has been widely utilized in optoelectronic applications such as an electrode material in organic photovoltaics (OPVs),[55-57] organic light-emitting diodes (OLEDs),[59] and sensors[60,61] due to its numerous advantages including a small bandgap (1.6–1.7 eV), low redox potential, good optical properties, high conductivity, and high processability from aqueous solution.[57,58] Recently, the PEDOT:PSS was used in nanocomposite with carbon nanotube (CNT) and GO to improve its optical and electrical properties.[62,63] Even though the optic and electrical properties of the nanocomposites were enhanced with CNT and GO, difficulty in preparation of the well dispersed carbon nanomaterials in water still remains. Herein, the PEDOT:PSS was utilized with GPN in water by simple sonication, followed by spin-coating on a glass substrate. The PEDOT:PSS/GPN thin film exhibited good dispersity of GPN in the PEDOT:PSS polymer matrix and improved electrical conductivity.

Experimental

Materials: Graphite powder (< 20 μm, synthetic, Sigma-Aldrich Inc.), sulfuric acid (H_2SO_4), hydrochloric acid (HCl), hydrogen peroxide (H_2O_2), potassium permanganate ($KMnO_4$), and sodium nitrate ($NaNO_3$) were purchased from Sigma-Aldrich Inc. $NMMO_m$ (which was evaporated from a 50 wt% aqueous solution of BASF© NMMO) was supplied by Kolon©. PEDOT:PSS (PH1000) (the solid content is 1 wt% in water) was purchased from Clevios™. Isopropyl alcohol (IPA) and sodium hydroxide (NaOH) were purchased from Junsei Chemical. Dimethyl sulfoxide (DMSO), dimethylformamide (DMF), ethanol, tetrahydrofuran (THF), dichloromethane (DCM), toluene, trichloroethylene (TCE), and *n*-hexane were obtained from Duksan Pure Chemicals Co., Ltd. (South Korea). All the chemicals were used as received.

Preparation of graphene: $NMMO_m$ (550 g) was melted at 90 °C in a cylindrical tube (diameter of 6 cm and length of 20 cm). After melting, the graphite powders (3 g, 0.54 wt%) were placed into the tube, and then, the tip of a horn-type sonicator (VCX-750, Sonics & Materials, Inc. Vibracell™, USA, 750 W and 20 Hz) was inserted into the tube. For 2 h, the NMMO/graphite mixture was sonicated at 90 °C. After sonication, the NMMO/graphite mixture was diluted with water (3 L). The diluted solution was left for 1 day to allow the supernatant and sediment parts to separate. The supernatant part was carefully decanted. The decanted part was centrifuged at 3,000 rpm for 30 min using a centrifuge (Vision Scientific Co., VS-21SMTN, Korea). Its supernatant part after centrifugation was subjected to a second centrifugation under the same conditions. After centrifugation and decanting, NaOH (2 g) was added to the supernatant part to precipitate the graphene. After 1 day, the precipitated graphene was filtered with large amounts of water (~ 3 L) on a cellulose filter (ADVANTEC®, cellulose membrane filter, 0.2-μm pore size) until the solution reached pH 7.

NMMO and NaOH were completely removed during filtration, and the black powders (GPN) could be gathered on the filter, which were dried in a vacuum oven at 60 °C.

Preparation of graphene film: The graphene film was prepared by a filtering method. The decanted solution before NaOH addition was filtered on a cellulose filter (ADVANTEC®, cellulose membrane filter, 0.2-μm pore size). The uniform free-standing film with a thickness of ~ 80 μm was peeled off to separate from the cellulose filter, and its electrical conductivity was measured using a four-point probe.

Dispersion in water: The aqueous dispersion of the GPN powders was performed using the tip of a horn-type sonicator (VCX-750, Sonics & Materials, Inc. Vibracell^{TM}, USA, 750 W and 20 Hz) with the aqueous solutions having designated GPN concentrations. All the experiments were performed with 2-h sonication unless otherwise noted. After sonication, the supernatant part was decanted, and its concentration was measured using a UV-Vis spectrometer (V-650, Jasco, Japan) from UV absorbance using the Lambert-Beer law with an absorbance coefficient of 38.008 mL/mg/cm (at 600nm), which was determined from a calibration curve.

Preparation of PEDOT:PSS/GPN nanocomposite: To obtain maximum electrical conductivity of the spin-coated PEDOT:PSS film on the glass substrate, the reported method was employed with IPA and ethanol treatments.[64,65] The procedure for the preparation of PEDOT:PSS/GPN nanocomposite thin films on the glass substrate with IPA mixing and ethanol soaking is described in the following text. The aqueous PEDOT:PSS solution (20 g, 1 wt%) was mixed with IPA (5 g) to obtain a 0.8 wt% PEDOT:PSS solution. Then, the predetermined amounts of GPN were added into the PEDOT:PSS/IPA solutions. The

PEDOT:PSS/IPA/GPN mixtures were vigorously stirred for 1 day with a magnetic bar and were then sonicated for 2 h using a horn-type sonicator. The sonicated PEDOT:PSS/IPA/GPN solutions were further stirred at 400 rpm for 1 day with a magnetic bar. Then, 0.3 mL of the final PEDOT:PSS/IPA/GPN solutions was spin-coated on the glass substrate in 3 steps (step 1 at 500 rpm for 5 sec, step 2 at 2,000 rpm for 20 sec, and step 3 at 800 rpm for 5 sec).[66] The spin-coated PEDOT:PSS/IPA/GPN films were dried at 80 °C on a hot plate for 1 min, and then, 0.5 mL of ethanol was dropped onto the spin-coated PEDOT:PSS/IPA/GPN thin film. The ethanol-soaked PEDOT:PSS/IPA/GPN film was left for 5 min with a glass dish cover and dried at 80 °C on a hot plate.[67] The prepared thin films were ~ 40 nm thick.

Preparation of GO: GO was synthesized by oxidizing graphite using the Hummer's method.[14] Briefly, 4 g of raw graphite, 2 g of $NaNO_3$ and 12 g of $KMnO_4$ were added to a 500-mL round-bottom flask containing 100 mL of concentrated H_2SO_4. The mixture was first cooled by immersion in an ice bath for 1 h with constant stirring and then slowly heated to 35 °C for 3 h. The reaction was quenched by adding 200 mL of deionized (DI) water, and the mixture was left to stand for 30 min. A H_2O_2 solution (30 %; 3 mL) was then added to reduce the unreacted permanganate. The mixture was then filtered through a cellulose filter and washed sequentially with dilute HCl and DI water. The resulting GO was dried at 60 °C for 48 h.

Characterization of graphene: A sonicated dilute aqueous GPN solution (0.001 mg/mL, 2 mL) was spin-coated at 1,000 rpm on the O_2 plasma-treated silicon wafer and dried completely for scanning electron microscopy (SEM, S-4800, Hitachi, Japan) and atomic force microscopy (Nanoscope IIIa, DI instrument, UK) observations. The powder samples were used for X-ray photoelectron spectroscopy (XPS, VG Microtech, ESCA2000, UK) using an

Al Kα X-ray source (1486.6 eV) in the range of 0 to 800 eV. The sheet resistance of the spin-coated films and electrical conductivity of the free-standing graphene film at room temperature were measured using a four-point probe in combination with a source meter (2400, Keithley, USA). Fourier-transform infrared spectroscopy (FTIR, FT/IR-620 unit, Jasco, Japan) was performed under vacuum. The FT-IR samples were vacuum-dried for 1 day, mixed with KBr, and pressed into 13-mm-diameter pellets. The spectra with a 1 cm^{-1} resolution were derived from 50 scans. Raman spectroscopy at 600 to 4000 cm^{-1} was performed using a Raman spectrometer (NT-MDT, NTEGRA spectra, Russia) with backscattering geometry and excitation at 532 nm of an argon laser. The WAXS experiments were performed using a Statton camera with an Anton-Parr X-ray generator operating at 40 kV and 50 mA, and a flat monochromator (Huber model 151) that produced Cu Kα radiation. Two-dimensional WAXS patterns recorded on phosphor image plates were scanned using an image reader (PerkinElmer, Cyclone). The sample-to-detector distance was calibrated using SiO_2 powders. The transmittance of the aqueous GPN solutions and spin-coated PEDOT:PSS/GPN films were measured using a UV/Visible spectrophotometer (V-650, Jasco, Japan). The zeta potential and size of GPN in water were measured with a dynamic light scattering instrument (ZEN3690, MALVERN, UK) at a 0.001 mg/mL concentration. The stability of the GPN dispersions in water was determined using Turbiscan (Turbiscan™ Lab Expert, Formulaction©, France) with the GPN aqueous solutions (0.001 mg/mL) sonicated for 2 h by a horn-type sonicator before the measurements. The solution transmittance for Turbiscan was measured along the vial height (range 5 to 35 mm) at λ = 880 nm every 30 min for 1 day and then every 1 day. The transmittance along the height at a certain time was averaged to obtain a graph of the transmittance as a function of time. Scanning transmission electron microscopy (STEM, Titan G2 ChemiSTEM Cs Probe, FEI, Netherlands) was performed at 200 kV to obtain the GPN images with selected area electron diffraction

(SAED) of the drop-cast samples of the aqueous solutions (0.001 mg/mL) on lacey carbon grids (TED PELLA, Inc., 200 mesh, Cu). The colloidal dispersion was studied with a He-Ne laser beam at 632.8 nm to observe the Tyndall effect.

Results and discussion

Preparation of water-dispersible graphene using $NMMO_m$:

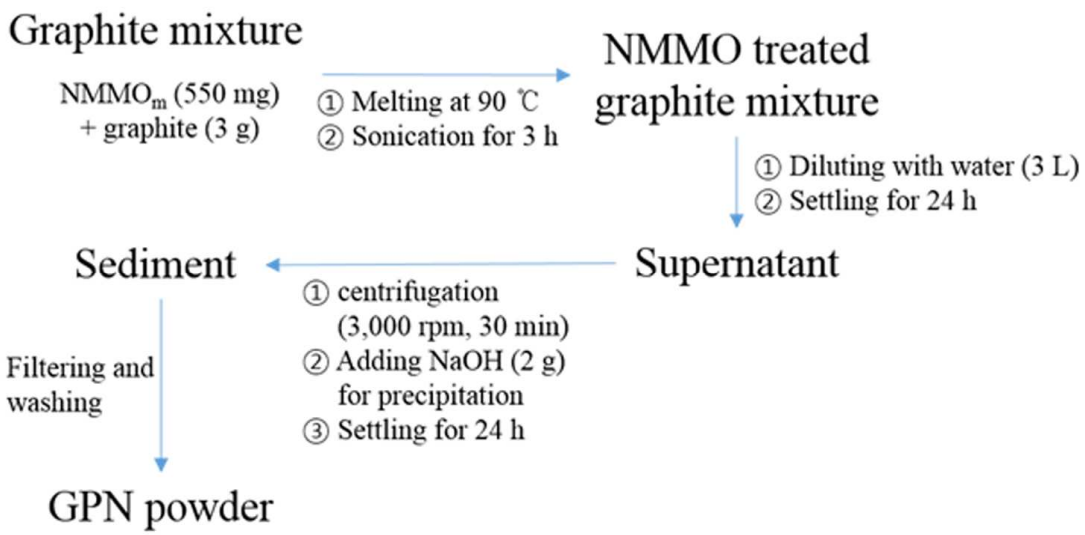

Scheme 1. Preparative procedure for water-dispersible graphene (GPN) using $NMMO_m$.

Scheme 1 shows the preparative procedure of GPN. The surface tension of $NMMO_m$ is known to be 44 mJ/m^2 at 80 °C,[68] which is close to the reported value of graphene (40–50 mJ/m^2), as discussed in the introduction. The close match of the surface tension between graphite and $NMMO_m$ can cause complete wetting of NMMO on the graphite surface and promote insertion of the NMMO molecules into the gallery of graphite to produce exfoliated graphene sheets. Graphene layers close to the outside surface of graphite contacting the $NMMO_m$ solution are easier to separate from graphite than the graphene layers inside the graphite; thus, although whole graphene sheets cannot be exfoliated from graphite, a limited

portion of the graphene layers can be separated from graphite in the $NMMO_m$ solution. To maximize the inclusion of NMMO in the gallery gaps of graphite, sonication was applied to the graphite solution in $NMMO_m$ at 80 °C. To collect the exfoliated graphene, a large amount of water was poured into the $NMMO_m$ solution because the sonicated graphite solution in $NMMO_m$ was solidified at room temperature without dilution of water; NMMO with hydration of more than 2.5 water molecules is known to be a liquid state below 40 °C. After sonication and dilution with water, only graphene (or few-layered graphene) could float in water, and graphite having many stacked layers precipitated on the bottom of the vial due to gravity after 1 day. The supernatant part was easily decanted. To obtain more pure graphene, the decanted part was centrifuged, and its supernatant part was collected again. The supernatant part was observed to be difficult to filter with a cellulose filter because the small-sized graphene could easily clog the filter. To solve this problem, NaOH was added to cause the precipitation of the supernatant. The zeta potential value of the aqueous GPN solution (0.001 mg/mL) was observed to be - 47.2 mV due to the small amounts of attached NMMO on the GPN surface, which will be discussed later. The addition of NaOH in the GO solution has been previously used by other scientists to precipitate GO for filtration purposes.[69,70] The Na^+ ions can form a complex with the negatively charged GPN such that the electrostatic repulsions between the GPN sheets were screened. The precipitated GPN powders were collected on the filter with a lot of water to wash away any residual NMMO and Na^+ ions. The collected GPN powders were dried in an oven at 60 °C for 1 day.

Dispersity of GPN in water:

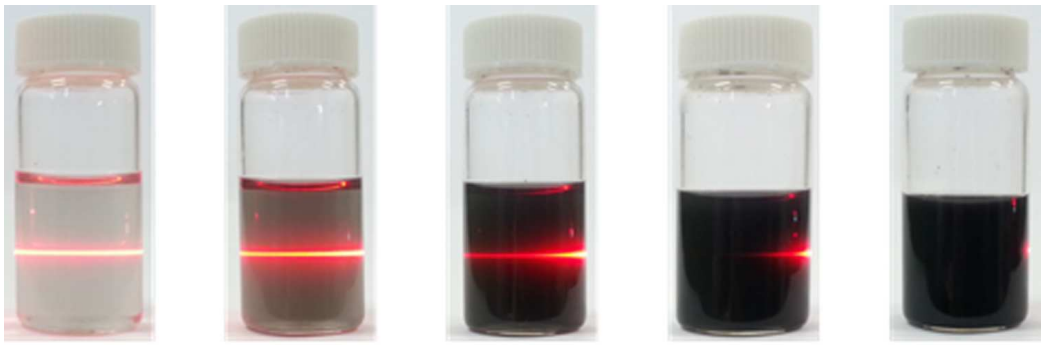

Figure 2. Photographic images of the dispersion of GPN in water after sonication for 2 h with different concentrations (C_{GPN}) of (a) 0.001, (b) 0.01, (c) 0.1, (d) 1, and (e) 3 mg/mL; the laser beams in the vials are used to observe the Tyndall effect.

Re-dispersion of the dried GPN powders in water was performed. Re-dispersion of dried powers has many merits because the exact amount of the GPN in a solvent can be controlled by weight (not by the volume of the solution). In addition, the solid-state GPN powders are more convenient to store than GPN in the solution state. Figures 2 a-e show photographs of the dispersion of GPN in water after sonication for 2 h with different concentrations (C_{GPN}) until 3 mg/mL. The black color is observed for the aqueous GPN solution (instead of the brown color of the aqueous GO solution) and becomes darker as C_{GPN} increases. No sediment was visible on the bottom of the vial. The clear straight laser beams in the vials due to the Tyndall effect indicate that the colloidal particles of the GPN were dispersed well in the water.[4] At high C_{GPN}s greater than 1 mg/mL, the GPN solution becomes so dark that the laser beam cannot be observed. The GPN solution at C_{GPN} = 0.001 mg/mL (the lowest concentration) shows no visible precipitation 1 day after sonication, whereas that at C_{GPN} = 0.1 mg/mL (the highest concentration) exhibits slight precipitation with the

supernatant remaining black. Figure SI 2 presents photographs of the GPN dispersion in water at C_{GPN} = 1 mg/mL immediately and 3 months after sonication for 2 h. The good dispersion still lasts with small amounts of precipitation, indicating that the dispersion of the GPN in water is stable for a long period.

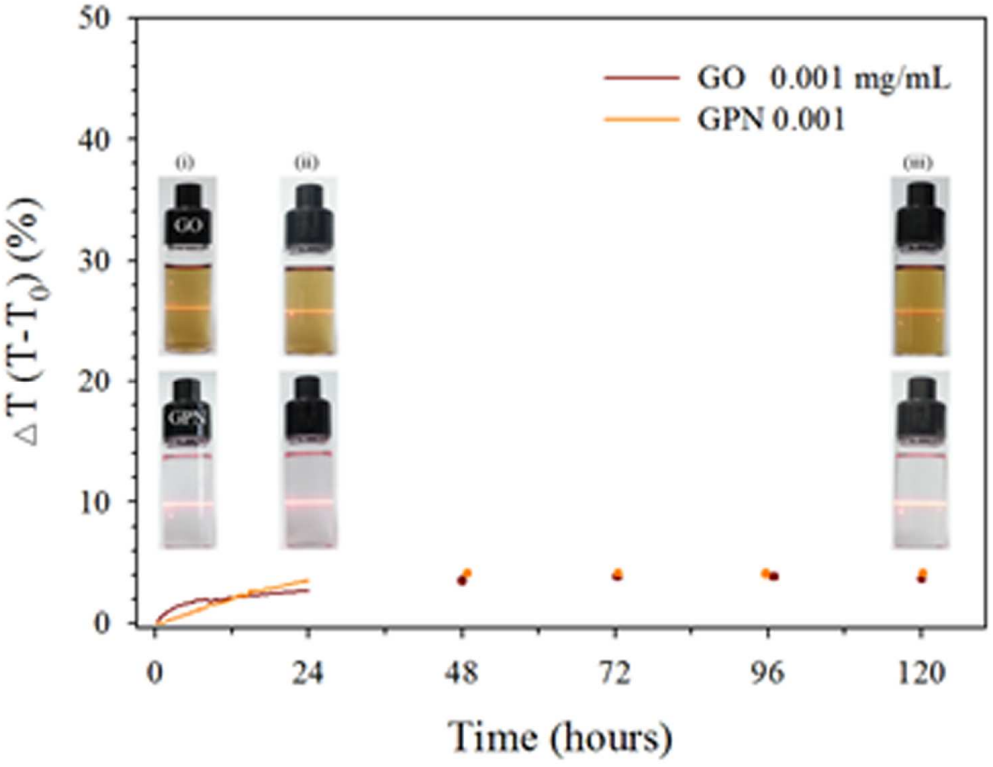

Figure 3. Transmission increases (ΔT) of the GPN and GO dispersions measured by Turbiscan as a function of time for 5 days with 0.001 mg/mL of C_{GPN} and C_{GO} (before 1 day : every 30 min, after 1 day : every 1 day), and (inset) photographs of the GPN and GO (i) immediately and (ii) 1 day and (iii) 5 days after sonication for 2 h; the laser beams in the vials are to see the Tyndall effect.

To quantitate the dispersion of the GPN, Turbiscan was used. The initial transmittances of the GPN and GO dispersions decrease as C_{GPN} and C_{GO} increase because of the absorption of

the beam by the GPN and GO particles. The GPN and GO dispersions at ≥ 0.1 mg/mL could not be tested because of the complete blocking (no transmission) of the beam resulting from the high concentration of the solution. The increase of the transmittance (ΔT, $T-T_0$) at a certain period represents the settlement of the particles; thus, a small increase of transmittance indicates stable dispersion of the particles in the solvent during that time. Figure 3 shows ΔT for 5 days (before 1 day : every 30 min, after 1 day : every 1 day) for the GPN and GO dispersions. ΔT of the GPN (and GO) dispersions increases slightly. However, ΔT of the GPN solution is comparable to that of the GO solution, indicating that the GPN exhibits similar dispersity in water as the GO even though there are few chemical functional groups in GPN, which will be discussed later.

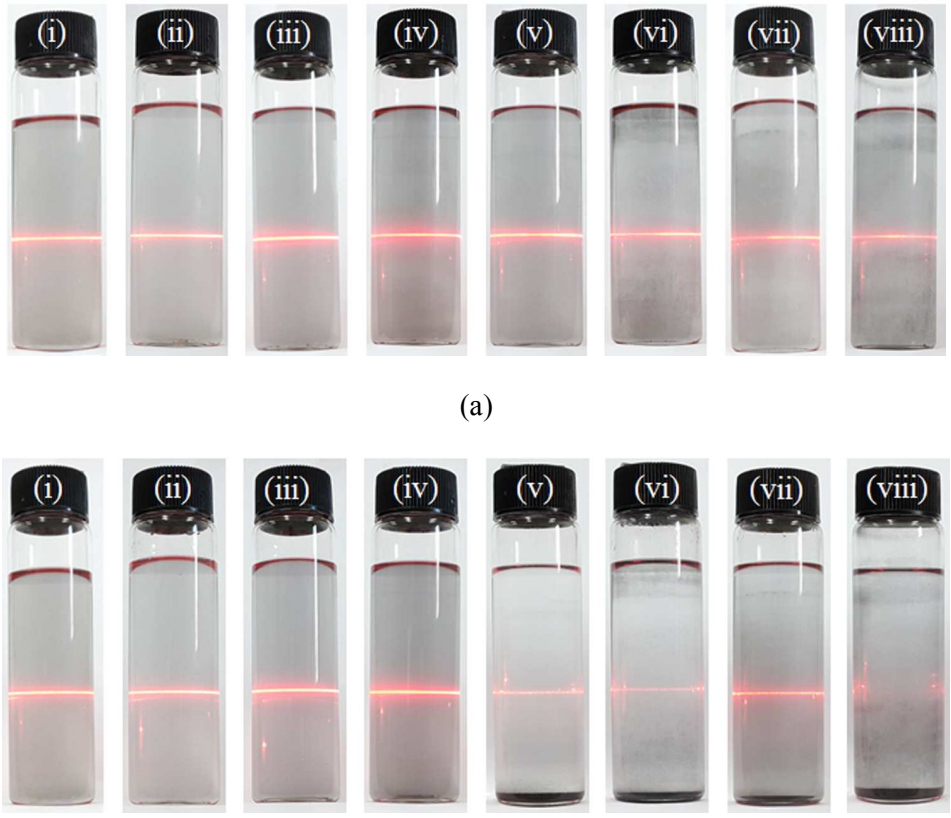

Figure 4. Photographs of the GPN dispersion at C_{GPN} = 0.001 mg/mL in (i) DMSO (7.2), (ii) DMF (6.4), (iii) ethanol (5.2), (iv) THF (4.0), (v) DCM (3.1), (vi) toluene (2.4), (vii) TCE (1.1), and (viii) *n*-hexane (0.0) (a) immediately and (b) 1 day after sonication for 2 h; the number in parenthesis is the polarity index ; the laser beams in the vials are to see the Tyndall effect.

The GPN dispersion was tested in several organic solvents. The GPN at C_{GPN} = 0.001 mg/mL was dispersed in different organic solvents by a horn-type sonicator. Figure 4 presents photographs of the GPN dispersion at C_{GPN} = 0.001 mg/mL in DMSO, DMF, ethanol, THF, DCM, toluene, TCE, and *n*-hexane immediately and 1 day after sonication for 2 h. For the GPN dispersion immediately after sonication for 2 h, the GPN in all the organic solvents was dispersed, which was evidenced by the black color and clear laser beam. However, 1 day

after sonication, the GPN in DCM, toluene, TCE, and *n*-hexane shows the settlement of GPN even though the GPN in DMSO, DMF, ethanol, and THF still shows good dispersion. The polarity indices of water, DMSO, DMF, ethanol, THF, DCM, toluene, TCE, and *n*-hexane are 9.0, 7.2, 6.4, 5.2, 4.0, 3.1, 2.4, 1.1, and 0, respectively.[71] This result indicates that the polar solvents such as water, DMSO, DMF, ethanol, and THF can disperse the GPN, which might be due to the high polar nature of the GPN powders. The dipole-dipole interactions between GPN and the polar solvent might improve the dispersity of the GPN in the solvents. The origin of the high polarity of GPN is not certain, although the small amounts of NMMO remaining on the GPN after the NMMO treatment might result in a large dispersion effect in the solvent at this moment. The existence of small amounts of NMMO on the GPN will be discussed later. Water is the most polar solvent; thus, the GPN is highly dispersible in water. The aqueous GPN solution at C_{GPN} = 0.001 mg/mL shows good dispersity with a zeta potential value of - 47.2 mV. According to the American Society for Testing and Materials (ASTM), colloids with zeta potentials higher than 40 mV (negative or positive) are known to have good stability in water.[72] Thus, polar-solvent-dispersible (more specifically, water-dispersible) GPN was generated with treatment of $NMMO_m$.

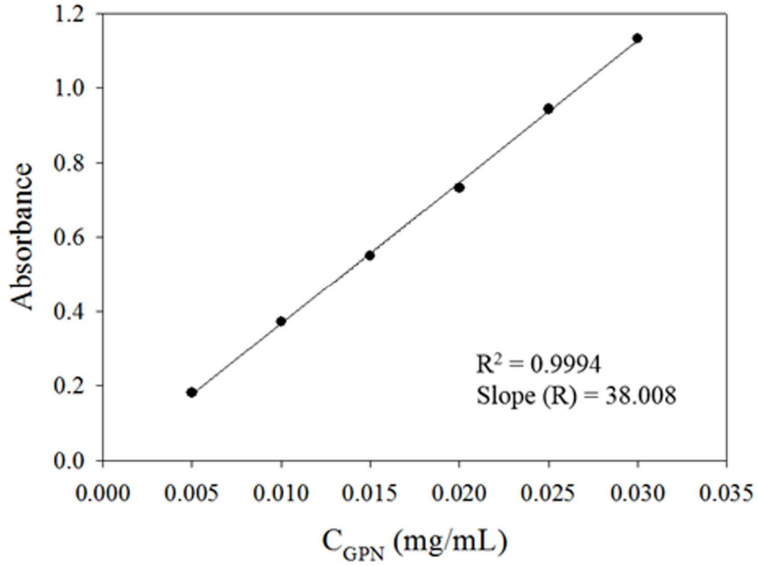

(a)

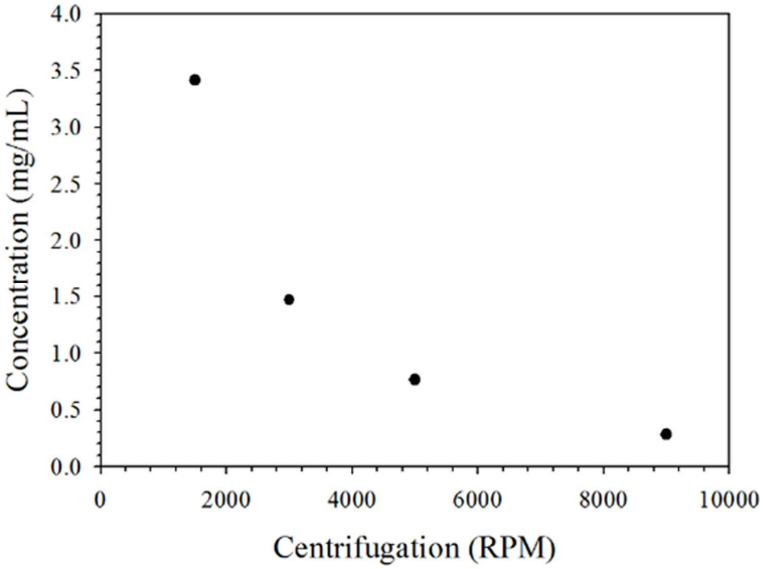

(b)

Figure 5. (a) UV−Vis absorbance of the aqueous GPN solution at 660 nm as a function of C_{GPN} immediately after sonication for 2 h, (b) the measured concentration from UV-Vis spectroscopy after centrifugation of the 5 mg/mL GPN solution for 10 min as a function of rpm; the data at 1,500 and 3,000 rpm were obtained from × 10 dilution with water after centrifugation.

The measurement of the amount of dispersible GPN in water is important. UV-Vis spectroscopy is commonly used to evaluate the amount of dispersible GPN in water. Coleman et al. studied the dispersion of NMP-treated graphene in NMP with centrifugation.[73] UV-Vis spectroscopy in the range of 0.005 to 0.03 mg/mL was performed to obtain a calibration curve. Figure SI 3 presents the UV-Vis spectra for different C_{GPN}s. These dilute GPN solutions show no precipitation without saturation at 660 nm in the UV-Vis spectra. The intensities of the spectra increase as C_{GPN} increases. Figure 5a shows the intensity at 660 nm as a function of C_{GPN}, representing a calibration curve. The straight line was obtained with good linearity (R^2=0.9994). The slope gives an absorption coefficient, α, of 38.01 mL/mg/cm in the Lambert-Beer equation. This value is quite close to the reported value (36.2 mL/mg/cm) of NMP-treated graphene in NMP studied by Coleman et al.[73-75]

The kinetics of the settlement of the dispersed graphene is one of the important considerations for disperse graphene from GPN powders because the settlement of graphene is dependent on the sizes (or number of stacks) of graphene. Centrifugation can accelerate its settlement, and the rpm can control the kinetics of the settlement. To evaluate the settlement of the dispersed GPN in water, centrifugation of the concentrated GPN solution (5 mg/mL) was performed at different rpms up to 9000 rpm (the highest level in the used centrifuge). Figure SI 4 presents the UV-Vis spectra at different rpms. This highly concentrated sonicated GPN solution before centrifugation has a black color, and its UV-Vis spectrum shows the saturation. After centrifugation at 1,500 and 3,000 rpm, the GPN solutions were still black and also resulted in saturation in the UV-Vis spectra. Thus, we diluted the centrifuged GPN solution 10 times with water and obtained UV-Vis spectra without saturation. Then, the concentrations of the solutions were calculated with the obtained absorption coefficient from Figure 5a using the Lambert-Beer law. The initial concentration before dilution was calculated by multiplying by 10. After centrifugation at high speeds of 5,000 and 9,000 rpm,

the GPN solutions became transparent without dilution and produced no saturation in the UV-Vis spectra such that the concentrations of the solutions were calculated directly with the same absorption coefficient using the Lambert-Beer law. Figure 5b shows the measured concentration of the aqueous GPN after centrifugation as a function of rpm. The concentration decreases exponentially as the centrifugation speed increases. The initial concentrated aqueous GPN solution (5 mg/mL) after sonication for 2 h may contain graphene sheets with a large distribution in the number of stacks in graphene. Many-stacked graphene will be settled at low rpm and little-stacked graphene will be settled at high rpm such that the amount of the settlement increases with increasing rpm of the centrifugation. The C_{GPN} values were 3.415, 1.468, 0.766, and 0.284 mg/mL after centrifugation at 1,500, 3,000, 5,000, and 9,000 rpm, respectively. Shulin et al. reported dispersion concentrations of 0.21 and 0.03 mg/mL in a water/acetone mixture from a water/acetone mixture-treated graphene after sonication for 12 h in a sonic bath with centrifugation at 500 and 4,000 rpm, respectively.[76] Coleman et al. reported dispersion concentrations of 0.1 and 0.05 mg/mL from NMP-treated graphene in NMP after sonication for 168 h in a sonic bath with centrifugation at 500 and 4000 rpm, respectively.[77] Thus, GPN can be more dispersible in water than NMP-treated graphene in NMP.

Structures of GPN:

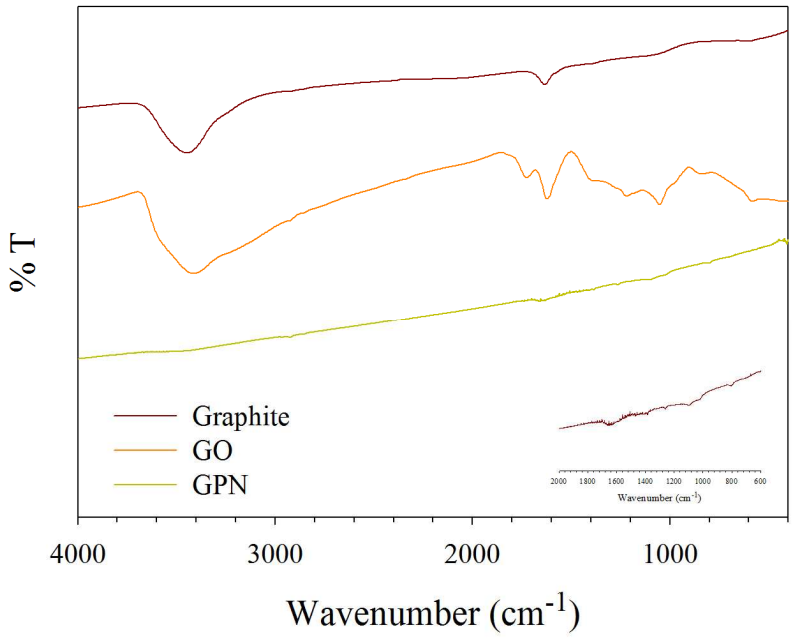

(a)

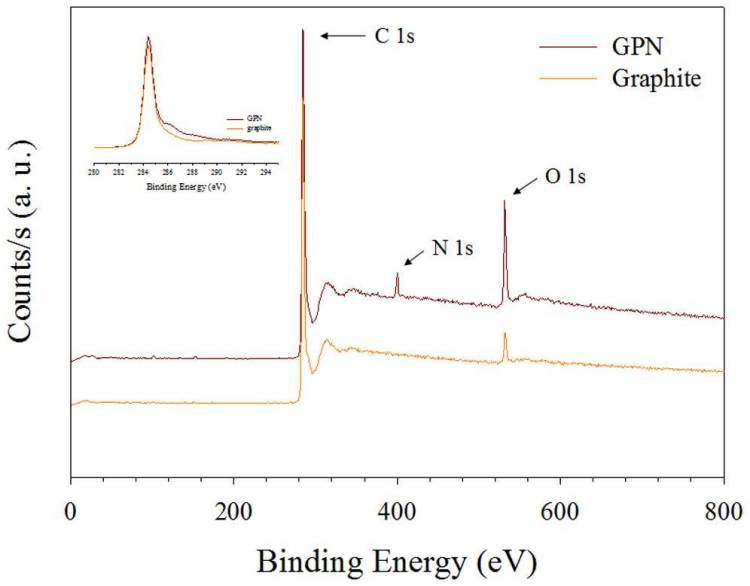

(b)

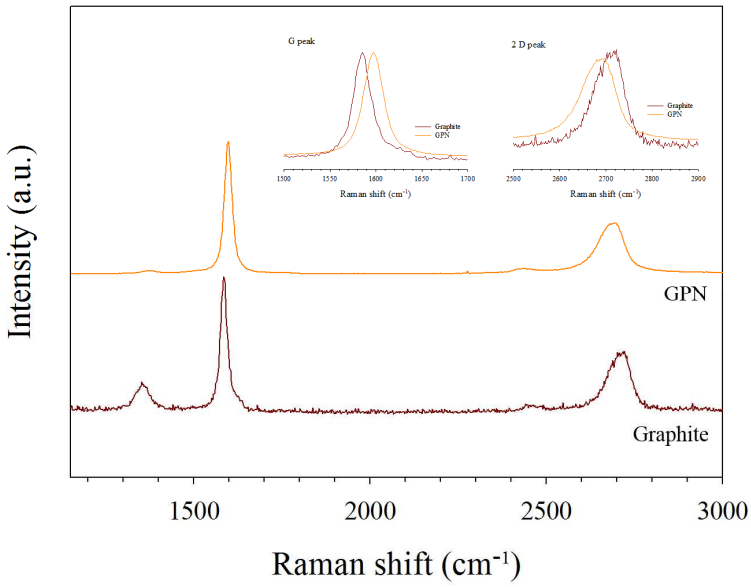

(c)

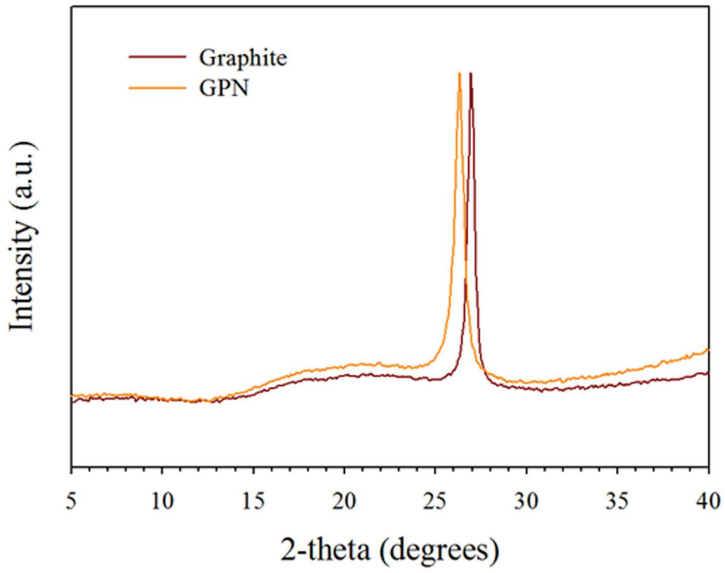

(d)

Figure 6. (a) FT-IR (inset: enlarged GPN spectrum below 2,000 cm^{-1}), (b) XPS (inset: enlarged C1s peak), (c) Raman spectra (inset: enlarged G and 2D peaks), and (d) WAXS patterns of the GPN and graphite samples; the GPN sample for Raman spectroscopy was prepared by spray-coating on the silicon wafer and the monolayer (or a few layers) of the GPN sample was confirmed by AFM.

The structure of GPN was analyzed by FT-IR, XPS, and Raman spectroscopies, as shown in Figure 6. The FT-IR spectrum of the GPN powders (Figure 6a) shows no discernible bands, suggesting that the GPN produced contained almost no functional groups as well as manifesting a complete graphene structure. However, the enlarged spectrum shows several small peaks which may be due to the small amounts of the remaining $NMMO_m$ although the detail study is necessary for assigning the peaks. The XPS spectrum of the GPN powders (Figure 6b) exhibited a strong C 1s peak and two small N 1s and O 1s peaks. The N 1s peak was assigned to residual NMMO molecules trapped on the GPN sheet. The N, O, and C contents in the GPN were 3.46, 11.05 and 85.49 wt%, respectively. An N atom combines with two oxygens and five carbon atoms in NMMO, such that the amounts of O and C atoms from NMMO were 7.91 and 14.83 wt%, respectively, and the amounts of O and C atoms from sources other than NMMO were 3.14 and 70.66 wt%, respectively. Therefore, the C/O ratio for GPN was 22.5 after excluding the NMMO O and C atoms. Graphite itself is known to contain a small amount of oxygen atoms due to air oxidation, as shown in Figure 6b, which is consistent with other reported results.[78] Thus, the C/O ratio (22.5) would increase after exclusion of the oxygen atoms that do not participate in the structural defects. The small amount of oxygen observed in GPN indicates that the material produced had a near defect-free graphene structure. The perfect graphitic structure can be confirmed by the C1s XPS spectrum (Figure 6b inset). The graphitic carbon (C–C) and nitrogen-bonded carbon (C-N) can be observed at 284.3 and 286.2 eV, respectively. The small C-N peak is due to the remaining NMMO. However, the carbon peaks related to oxidization typically associated with GO[44,79] are not observed. These experiments again confirm that high-quality, unoxidized graphene flakes can be produced with NMMO treatment. The Raman spectrum of the GPN (and graphite) samples (Figure 6c) shows sharp D, G and 2D peaks at 1359 (1370), 1598

(1585) and 2689 (2721) cm^{-1}, respectively; the numbers in parentheses are the data for graphite. The GPN sample for Raman spectroscopy was prepared by spray-coating on the silicon wafer and the monolayer (or a few layers) of the sample was confirmed by AFM. The G peak is much higher than the D peak. The existence of the 2D peak of the GPN sample with its symmetrical shape also indicates that the structure of GPN is close to that of graphene without defects. The presence of a D band in the graphite powders was attributed to the small Raman excitation beam size used.[19] Thus, observance of the D peak in the spectrum of the GPN may be due to the same reason. The G and 2D peaks of GPN were blue- and red-shifted compared with those of graphite powder, respectively (Figure 6c inset). The observed blue shift of the G peak and the red-shift of the 2D peak of the GPN sample compared with that of the graphite powder was attributed to the monolayer (or a few layers) of the graphene sheets.[80] Thus, the Raman spectrum of GPN was similar to that of the graphite powders, except for a slight peak shift, indicating that the structure of the produced GPN was similar to that of the graphite layer. The gallery gap in the GPN powder was examined by WAXS, as shown in Figure 6d. The WAXS pattern of the GPN powder shows a peak at $2\theta = 26.30°$ (d-spacing= 3.39 Å), which was down shifted from that of graphite ($2\theta = 26.94$ ° (d-spacing= 3.31 Å)). The increased gallery gap in GPN compared to graphite was probably due to the entrapment of the remained NMMO between the GPN sheets. The FT-IR, XPS, Raman spectroscopy, and WAXS studies strongly indicate that the structure of the produced GPN is close to that of graphene without defects.

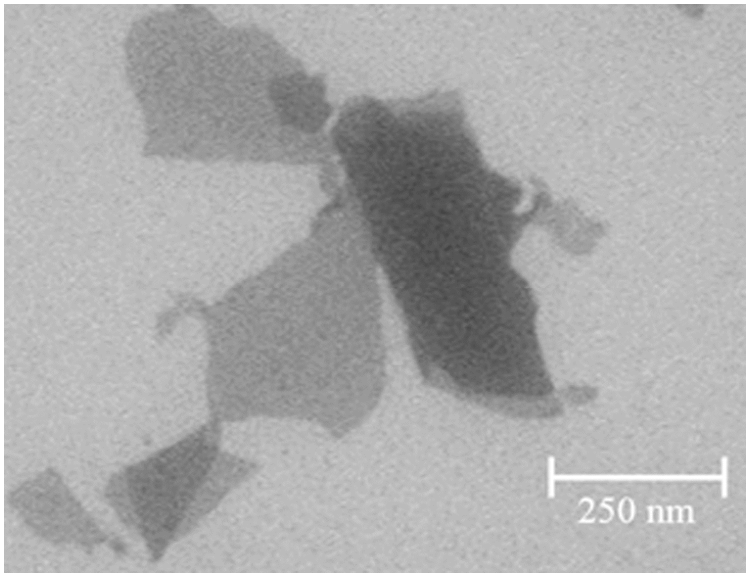

(a)

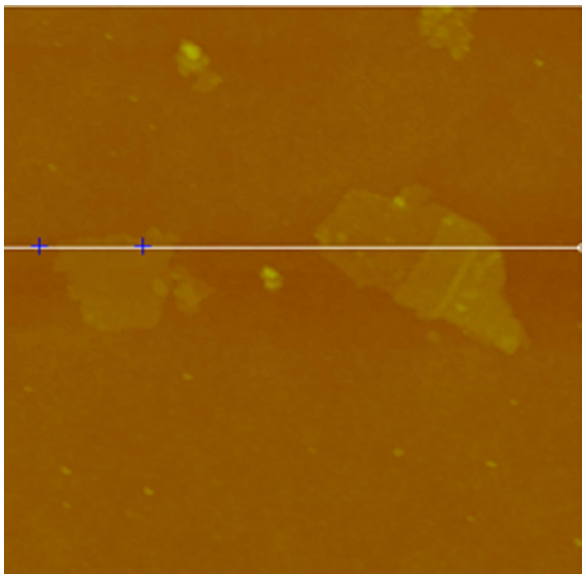

(b)

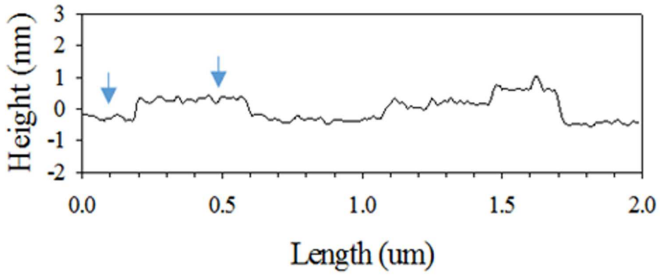

(c)

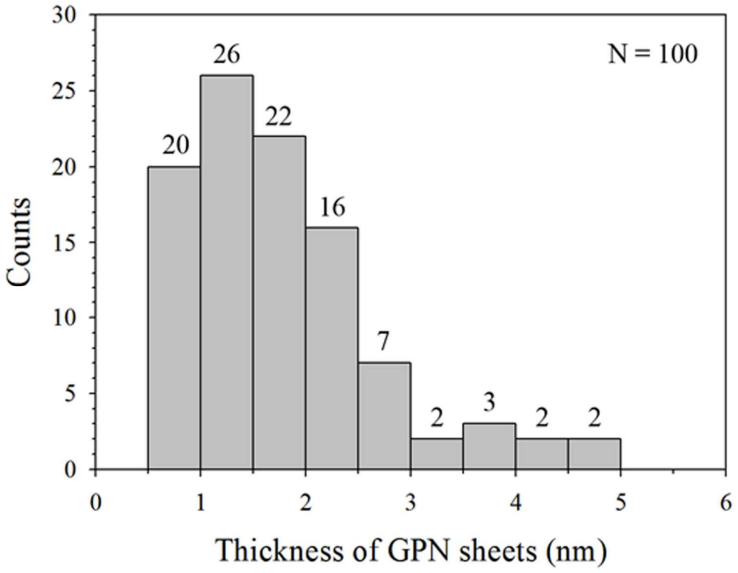

(d)

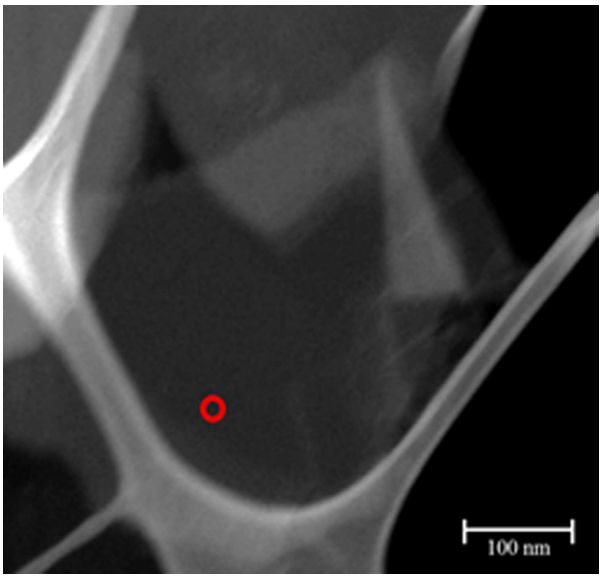

(e)

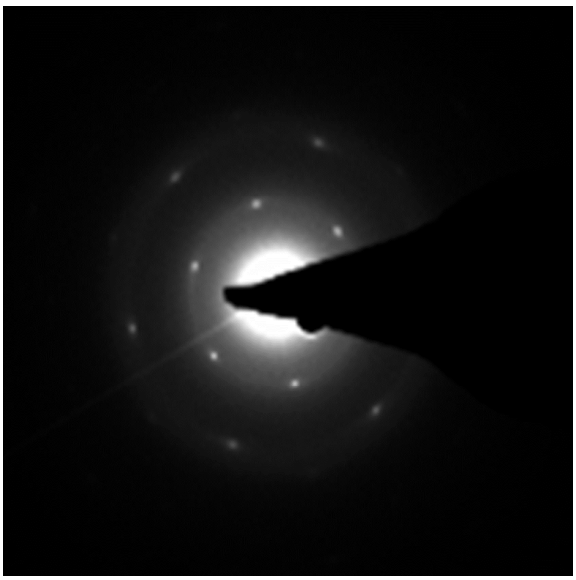

(f)

Figure 7. (a) SEM and (b) AFM images of the GPN on a silicon wafer; (c) height profile of the line in (b); (d) thickness distribution for one hundred arbitrary graphene measured using AFM; (e) STEM image and (f) selective area electron diffraction (SAED) pattern of the single-layered graphene in the circled area in (e).

The morphology of the GPN was studied with SEM, AFM, and STEM, as shown in Figure 7. The samples for SEM and AFM were prepared by spin coating a dilute aqueous GPN dispersion (0.001 mg/mL) on a silicon wafer. The SEM image (Figure 7a) shows the semi-transparent and darker GPNs on the silicon water, which represent the single-layered and overlapped layered structures, respectively. The overlapped structure may be due to restacking and/or folding of the individual single-layered sheets during the sample preparation. The AFM image (Figure 7b) reveals a single-layered structure on the silicon wafer. The layered thickness from the height profile (Figure 7c) is ~ 0.6 nm, which is similar to the theoretical value of a single layer, and the length of the long axis of the GPN sheet is ~ 300 nm which is a typical size for sonicated samples.[81] Figure 7d shows a representation of

the observed distribution. It was found that > 90% of the graphene sheets had three or fewer layers, and the mean layer number per flake was two. Therefore, the GPN in water was exfoliated into single layers in dispersion by simple sonication. The single-layered structure was explored in more detail using STEM with electron diffraction. The transparent sheet on the STEM grid is clearly observed in Figure 7e. The SAED pattern (Figure 7f) of the circled area in Figure 7e shows the inner (1100) diffractions and next outer (2110) diffractions with a two-dimensional hexagonal symmetry.[11] The (1100) diffractions are stronger than the (2110) diffractions. The (1100) diffractions of the single-layered graphene sheet are known to be stronger than the next (2110) diffractions, and vice-versa for the multilayers.[18] Most of the observed SAEDs from other samples had stronger (1100) diffractions than (2110) diffractions. Several hexagonal patterns with different intensity distribution were also observed from other samples. For example, the SAED had stronger (2110) diffractions than (1100) diffractions at the multi-layered part, and the stacking of the individual sheet was not epitaxially matched, which resulted in overlapped electron diffractions with a certain tilting angle. (e.g., Figure SI 5). However, these patterns were rarely observed, indicating that most GPNs produced had the single-layered structure.

Electrical conductivity of graphene film: The electrical conductivity of the GPN film prepared by a filtering method was measured using a four-point probe. Its electrical conductivity was 94.7 S/cm. Samulski et al. reported electrical conductivities of 0.17, 12.5, and 61.2 S/cm from the sulfonated GO (GO-SO_3H, water-soluble), graphene, and graphite, respectively.[72] This high conductivity of 94.7 S/cm from GPN was due to the complete graphitic structure without defects, as mentioned for the FT-IR, XPS, and Raman spectroscopy results.

PEDOT:PSS/GPN nanocomposite:

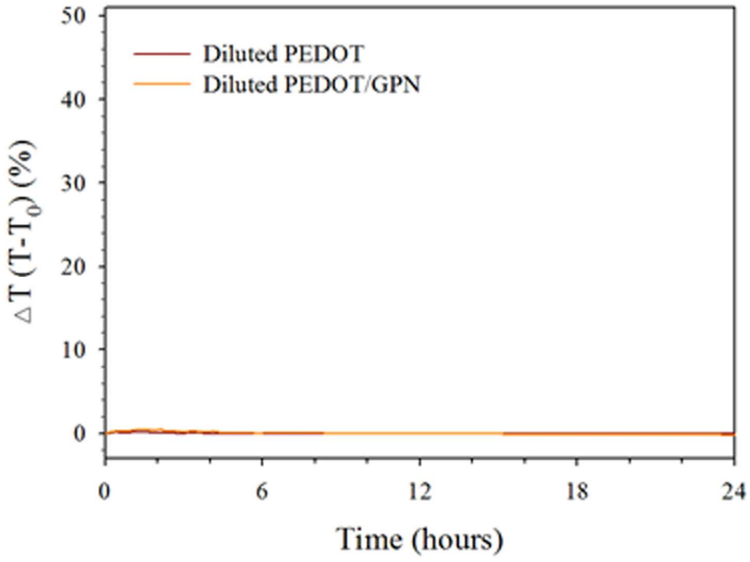

(a)

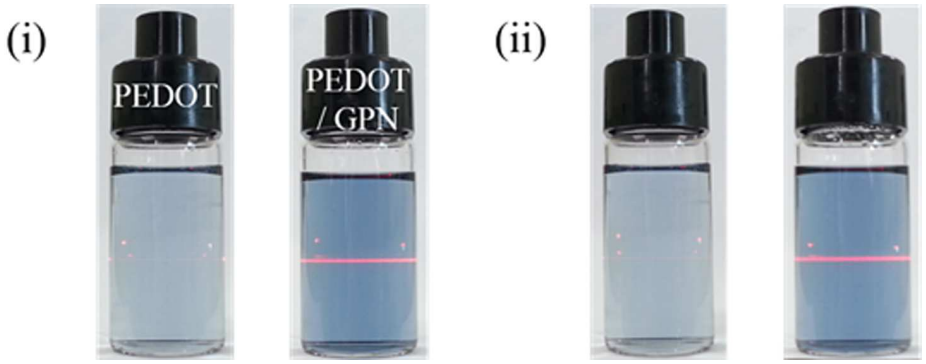

(b)

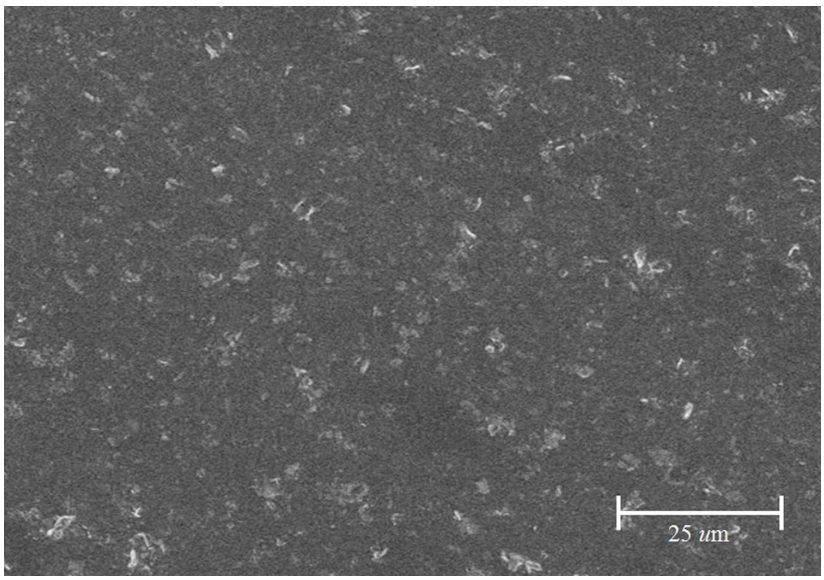

(c)

Figure 8. (a) Increase of the averaged transmissions ($\Delta T = T - T_0$) of the PEDOT:PSS and PEDOT:PSS/GPN (ϕ = 3 wt%) solutions after × 20 times dilution with water during 1 day. (b) Photographs of the vials containing the PEDOT:PSS and PEDOT:PSS/GPN (ϕ = 3 wt%) solutions (i) immediately and (ii) 1 day after × 20 times dilution with water; the laser beams in the vials are to see the Tyndall effect. (c) SEM image of the PEDOT:PSS/GPN (ϕ = 3 wt%) from the sample prepared by drop-casting of the × 20 water-diluted solution on a silicon wafer and drying in an oven at 60 °C.

Water-dispersible GPN can find many applications for nanocomposites with water-soluble polymers. The aqueous PEDOT:PSS system was employed to demonstrate the improvement of the electrical properties by mixing with GPN. To study the dispersity of GPN in the aqueous PEDOT:PSS solution, the transmittance of the PEDOT:PSS/GPN solution was measured for 1 day using Turbiscan. Figure 8a shows the increase of the transmittance of PEDOT:PSS and PEDT:PSS/GPN (ϕ = 3 wt%, ϕ is the amount of GPN vs. the solid content of PEDOT/PSS) solutions after 20 times dilution with water; the

PEDOT:PSS aqueous solution was diluted because the initial (as-received) PEDOT:PSS and PEDOT:PSS/GPN (ϕ = 3 wt%) aqueous solutions were too dark to measure the transmittance. The transmittances of the PEDOT:PSS and PEDOT:PSS/GPN (ϕ = 3 wt%) aqueous solutions do not increase within experimental errors even after 1 day. A clear laser beam from strong Tyndall scattering was observed for the PEDOT:PSS/GPN (ϕ = 3 wt%) aqueous solution 1 day after mixing (Figure 8b), indicating that the GPN was well dispersed in the aqueous PEDOT:PSS solution. This facile preparation of the PEDOT:PSS/GPN solution can be used for the thin-film application by drop-coating. The drop coating on the silicon wafer as well as the bare glass was performed with 0.5 mL of the × 20 water diluted PEDOT:PSS/GPN solution and dried on a hot plate at 80°C. The prepared thin film on the silicon wafer was studied with SEM, as shown in Figure 8c. The GPN sheets extruded from the surface of the thin film are uniformly distributed on the surface of the thin film. The sizes of the extruded GPN sheets are ~ several hundred nm, which is close to the SEM and AFM results. This good dispersion of GPN in the PEDOT:PSS matrix may be due to the strong π-π interactions between aromatic rings of PEDOT and the GPN.

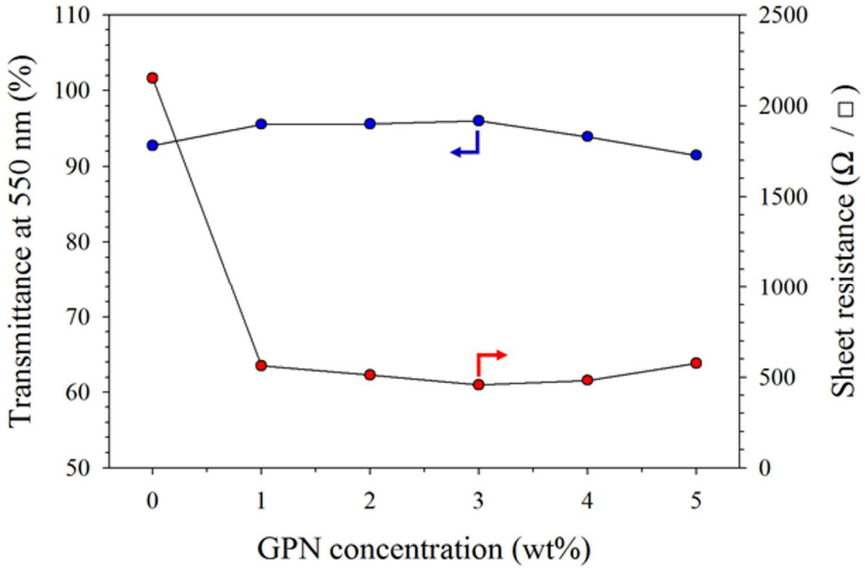

(a)

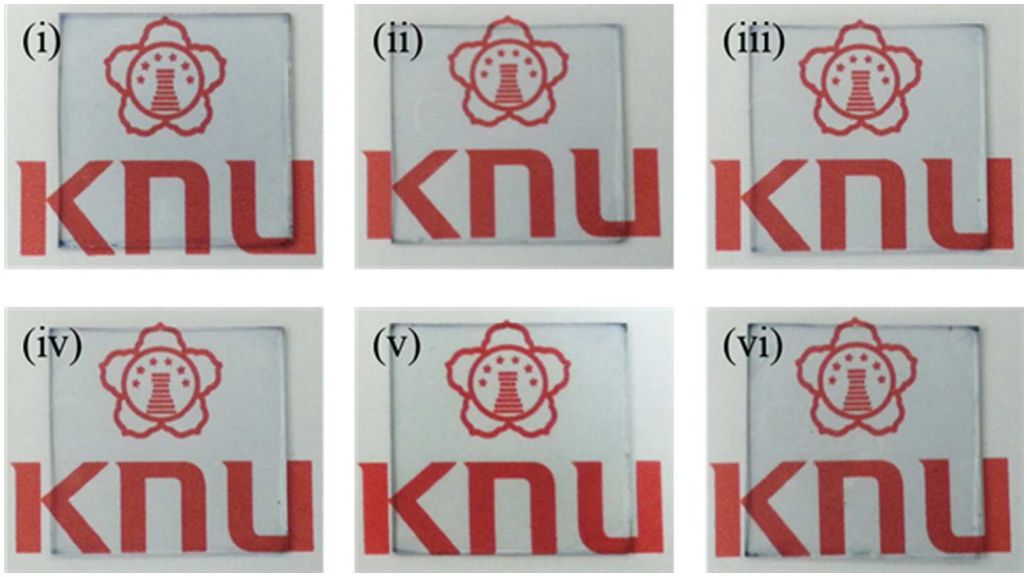

(b)

Figure 9. (a) (blue filled circle) Transmittances at 550 nm and (red filled circle) sheet resistances of the PEDOT:PSS/GPN nanocomposite thin films on a glass substrate as a function of ϕ; (b) images of the thin films at ϕ = (i) 0, (ii) 1, (iii) 2, (iv) 3, (v) 4, and (vi) 5 wt%.

The electrical conductivity and transmittance of the spin-coated film on the glass substrate were tested. The thin film of the PEDOT:PSS was prepared with IPA mixing and ethanol treatment because the electrical conductivity of the PEDOT:PSS thin film is known to increase with IPA mixing and ethanol soaking, as discussed in the experimental section.[64,65] Figure 9a shows the transmittance at 550 nm and the sheet resistance of the spin-coated PEDOT:PSS/GPN nanocomposite thin films on the glass substrate as a function of ϕ until 5 wt% at 1 wt% intervals. The thickness of the film was controlled at ~ 40 nm. The spin-coated films show no aggregation on the glass substrate with good transparency, indicating that all the PEDOT:PSS/GPN aqueous solutions exhibited a good coating

capability with good GPN dispersion. The sheet resistance of the pristine PEDOT:PSS (ϕ = 0 wt%) is 2,152 Ω/□ and decreases to 562.6, 511.8, 457.2, 482.4, and 576.3 Ω/□ at ϕ = 1, 2, 3, 4, and 5 wt%, respectively. The sheet resistance of the thin film of the PEDOT:PSS/GPN decreases substantially at ϕ = 1 wt% (562.6 Ω/□) from that of the pristine PEDOT:PSS (2,152 Ω/□), slightly decreases with further increase of the GPN until ϕ = 3 wt%, and then slightly increases. The sheet resistances of all the PEDOT:PSS/GPN thin films (at ϕ = 1, 2, 3, 4, and 5 wt%) are ~ 4 times lower than that of the pristine PEDOT:PSS thin film. This improvement of the electrical conductivity is due to the good dispersity of GPN in the aqueous PEDOT:PSS solution and the graphitic structure of GPN without defects. The good dispersion of the GPN in the aqueous PEDOT:PSS solution may be due to the π-π interactions between aromatic rings of PEDOT and graphene.[82] However, the decrease of the sheet resistance is not significant after ϕ = 1 wt%, and the minimum sheet resistance was observed at ϕ = 3 wt%. The difference in the sheet resistance between ϕ = 1 and 3 wt% is only 30 Ω/□, which might be due to the overlapping and aggregation of GPN in the PEDOT:PSS matrix. However, a more detailed study is necessary to determine the exact reasons for the slight decrease of the sheet resistance after ϕ = 1 wt%. The PEDOT:PSS/GPN thin films exhibit transmittances of 92.8, 95.5, 95.6, 95.9, 93.9, and 91.5 % at ϕ = 0, 1, 2, 3, 4 and 5 wt%, respectively. Figure 9b presents their transparent photo images on the KNU letters. The transmittances of the PEDOT:PSS thin films are not affected much at ~ 94 ± 2 % by the addition of GPN. The transmittance of the PEDOT:PSS thin films even increases with the addition of GPN until ϕ = 3 wt%. Several reasons, such as the matched refractive indices between GPN and PEDOT:PSS,[83] the decreased size of the PEDOT by sonication,[65] and/or the compensation of the blue color of PEDOT by the black color of GPN,[84] may explain the decrease of the transmittance. The transmittance decreases with further addition of GPN at ϕ

> 3 wt% most likely because of the aggregation of the GPN in the PEDOT:PSS matrix. However, the transmission levels are still high enough for transparent electrode applications. In this study, we observed a fourfold increase in the electrical conductivity of the PEDOT:PSS with the addition of 1 wt% GPN without deterioration of the transparency (and even a small improvement in the transparency).

Conclusion:

Environmentally friendly and non-toxic $NMMO_m$, which has a similar surface tension as graphite and a highly polar nature was found to be a good exfoliating solvent for graphite powders to make water-soluble solid-state GPN powders by sonication of the graphite in the $NMMO_m$ solution, dilution with water, decanting, filtration, centrifugation, and drying. Re-dispersion of the GPN solid powders in water by simple sonication.was successfully demonstrated. A high concentration (0.284 mg/mL) was obtained even after high-speed centrifugation at 9000 rpm for 10 min. The small amount of the remaining NMMO on GPN induced the strong negatively charged state in water (- 47.2 mV from the zeta potential) due to high polar nature of the NMMO, which may cause the electrostatic repulsions between them and dispersions in polar solvents. The produced GPN exhibited a single-layered graphitic structure without defects, which was studied with SEM, AFM, and STEM (with SAED). The electrical conductivity measured from a filtered GPN film was 94.7 S/cm. A well-percolated nanocomposite system with a water-soluble polymer blend was demonstrated with the aqueous PEDOT:PSS on the glass substrate. A fourfold increase in the electrical conductivity of PEDOT:PSS was achieved by adding 1 wt% GPN without deterioration of the transmittance. Thus, this water-dispersible GPN can find many applications in nanocomposites via its mixture with water-soluble polymers, and its spin coating ability opens in the path to device applications such as solar cells, organic light-

emitting devices, and touch screens.

Acknowledgments: Financial supports from the Asian Office of Aerospace Research and Developement through the Air Force Research Laboratory and the National Research Foundation of Korea (NRF-2011-0020264, NRF-2014R1A2A1A11050451) are gratefully acknowledged.

References

1. M. Segal, *Nature Nanotech*., 2009, 4, 612-614.

2. C. Lee, X. D. Wei, S. W. Kysar and J. Hone, *Science*, 2008, 321, 385-388.

3. A. A. Balandin, S. Ghosh, W. Z. Bao, I. Calizo, D. Teweldebrhan, F. Miao and C. N. Lau, *NanoLett*., 2008, 8, 902-907.

4. N. Behabtu, J. R. Lomeda, M. J. Green, A. L. Higginbotham, A. Sinitskii, D. V. Kosynkin, D. Tsentalovich, A. N. G. Parra-Vasquez, J. Schmidt, E. Kesselman, Y. Cohen, Y. Talmon, J. M. Tour and M. Pasquali, *Nature Nanotech*., 2010, 5, 406-411.

5. A. K. Geim, S. V. Morozov, D. Jiang, Y. Zhang, S. V. Dubonos, I. V. Grigorieva and A. A. Firsov, *Science*, 2004, 306, 666-669.

6. D. C. Wei, Y. Q. Liu, Y. Wang, H. L. Zhang, L. P. Huang and G. Yu, *NanoLett*., 2009, 9, 1752-1758.

7. J. H. Park, W. C. Mitchel, L. Grazulis, K. Eyink, H. E. Smith and J. E. Hoelscher, *Carbon*, 2011, 49, 631-635.

8. P. W. Sutter, P. M. Albrecht and E. A. Sutter, *Appl. Phys. Lett*., 2010, 97, 213101-213103.

9. R. Hao, W. Qian, L. H. Zhang and Y. L. Hou, *Chem. Commun*., 2008, 44, 6576-6578.

10. W. Qian, R. Hao, Y. L. Hou, Y. Tian, C. M. Shen, H. J. Gao and X. L. Liang, *Nano Res*., 2009, 2, 706-712.

11. M. J. McAllister, J. L. Li, D. H. Adamson, H. C. Schniepp, A. A. Abdala, J. Liu, M. Herrera-Alonso, D. L. Milius, R. Car, R. K. Prud'homme and I. A. Aksay, *Chem. Mater*., 2007, 19, 4396-4404.

12. S. Stankovich, D. A. Dikin, R. D. Piner, K. A. Kohlhaas, A. Kleinhammes, Y. Jia, Y. Wu, S. T. Nguyen and R. S. Ruoff, *Carbon,* 2007, 45, 1558-1565.

13. X. Cui, C. Z. Zhang, R. Hao and Y. L. Hou, *Nanoscale*, 2011, 3, 2118-2126.

14. W. S. Hummers and R. E. Offeman, *J. Am. Chem. Soc*., 1958, 80, 1339.

15. H. C. Schniepp, K. N. Kudin, J.-L. Li, R. K. Prud'homme, R. Car, D. A. Saville and I. A. Aksay, *ACS Nano*, 2008, 2, 2577-2584.

16. Q. Su, S. Pang, V. Alijani, C. Li, X. Feng and K. Mullen, *Adv. Mater*., 2009, 21, 3191-3195.

17. S. Pang, H. N. Tsao, X. Feng and K. Mullen, *Adv. Mater*., 2009, 21, 3488-3491.

18. Y. Hernandez, V. Nicolosi, M. Lotya, F. M. Blighe, Z. Y. Sun, S. De, I. T. McGovern, B. Holland, M. Byrne, Y. K. Gun'ko, J. J. Boland, P. Niraj, G. Duesberg, S. Krishnamurthy, R. Goodhue, J. Hutchison, V. Scardaci, A. C. Ferrari and J. N. Coleman, *Nat. Nanotechnol*., 2008, 3, 563-568.

19. M. Lotya, Y. Hernandez, P. J. King, R. J. Smith, V. Nicolosi, L. S. Karlsson, F. M. Blighe, S. De, Z. Wang, I. T. McGovern, G. S. Duesberg and J. N. Coleman, *J. Am. Chem. Soc*., 2009, 131, 3611-3620.

20. J. N. Coleman, *Adv. Funct. Mater*., 2009, 19, 3680-3695.

21. J. N. Coleman, *Acc. Chem. Res*., 2013, 46, 14-22.

22. X. Y. Zhang, A. C. Coleman, N. Katsonis, W. R. Browne, B. J. van Wees and B. L. Fering, *Chem. Commun.*, 2010, 46, 7539-7541.

22. A. B. Bourlinos, V. Georgakilas, R. Zboril, T. A. Steriotis and A. K. Stubos, *Small*, 2009, 5, 1841-1845.

23. M. Inagaki, Elsevier, Amsterdam, 2000, (2) M. Inagaki, *J. Mater. Res*., 1989, 4, 1560-1568.

24. Y. Sun, S. R. Wilson and D. I. Schuster, *J. Am. Chem. Soc*.,2001, 123, 5348-5349.

25. F. Zhang and Y. Fang, *J. Phys. Chem. B*, 2006, 110, 9022-9026.

26. W. Du, X. Jiang and L. Zhu, J. *Mater. Chem. A*, 2013, 1, 10592-10606.

27. X. Q. Wang, P. F. Fulvio, G. A. Baker, G. M. Veith, R. R. Unocic, S. M. Mahurin, M. F. Chi and S. Dai, *Chem. Commun*., 2010, 46, 4487-4489.

28. D. Nuvoli, L. Valentini, V. Alzari, S. Scognamillo, S. B. Bon, M. Piccinini, J. Illescas and A. Mariani, *J. Mater. Chem*., 2011, 21, 3428-3431.

29. Y. Hernandez, M. Lotya, D. Rickard, S. D. Bergin and J. N. Coleman, *Langmuir*, 2010, 26, 3208-3213.

30. A. O'Neill, U. Khan, P. N. Nirmalraj, J. Boland and J. N. Coleman, *J. Phys. Chem. C,* 2011, 115, 5422-5428.

31. E.-Y. Choi, W. S. Choi, Y. B. Lee and Y. –Y. Noh, *Nanotechnology*, 2011, 22, 365601.

32. S. Vadukumpully, J. Paul and S. Valiyaveettil, *Carbon*, 2009, 47, 3288-3294.

33. R. J. Smith, M. Lotya and J. N. Coleman, *New J. Phys.,* 2010, 12, 125008.

34. M. Lotya, P. J. King, U. Khan, S. De and J. N. Coleman, *ACS Nano*, 2010, 4, 3155-3162.

35. L. Guardia, M. J. Fern´andez-Merino, J. I. Paredes, P. Sol´ıs-Fern´andez, S. Villar-Rodil, A. Mart´ınez-Alonso and J. M. D. Tasc´on, *Carbon*, 2011, 49, 1653-1662.

36. A. B. Bourlinos, V. Georgakilas, R. Zboril, T. A. Steriotis, A. K. Stubos, C. Trapalis, *Solid State Communications*, 2009, 149, 2172-2176.

37. Y. Xu , H. Bai , G. Lu , C. Li and G. Shi, *J. Am. Chem. Soc.*, 2008, 130, 5856-5857.

38. M. Zhang, R. R. Parajuli, D. Mastrogiovanni, B. Dai, P. Lo, W. Cheung, R. Brukh, P. L. Chiu, T. Zhou, Z. Liu, E. Garfunkel and H. He, *Small*, 2010, 6, 1100-1107.

39. J. Guo, L. Ren, R. Wang, C. Zhang, Y. Yang and T. Liu, *Composites Part B: Engineering*,

2011, 42, 2130-2135.

40. G. S. Bang, H.-M. So, M. J. Lee and C. W. Ahn, *J. Mater. Chem*., 2012, 22, 4806-4810.

41. A. B. Bourlinos, V. Georgakilas, R. Zboril, T. A. Steriotis, A. K. Stubos, C. Trapalis, *Solid State Communications*, 2009, 149, 2172-2176.

42. C. Shan, H. Yang, D. Han, Q. Zhang, A. Ivaska and L. Niu, *Langmuir*, 2009, 12030-12033.

43. H. Bai, Y. Xu, L. Zhao, C. Li and G. Shi, *Chem. Commun*., 2009, 13, 1667-1669.

44. D. Li, M. B. Müller, S. Gilje, R. B. Kaner and G. G. Wallace, *Nature Nanotechnology*, 2008, 3, 101-105.

45. J. Gassan and A. K. Bledzki, *J. Appl. Polym. Sci*. 1999, 71, 623-629.

46. C. H. Kuo, and C. K. Lee, *Bioresource Technology*, 2009, 100, 866-871.

47. H.-P. Fink, P. Weigel, H. J. Purz and J. Ganster, *Prog. Polym. Sci*., 2001, 26, 1473-1524.

48. T. Rosenau, A. Potthast, H. Sixta and P. Kosma, *Prog. Polym. Sci*., 2001, 26, 1763-1837.

49. H. Chanzy, E. Maia and S. Perez, *Acta Cryst. B*, 1982, 38, 852-855.

50. C. Michels and B. Kosan, Lenzinger Berichte 2005, 84, 62-70.

51. L. X. Benedict, N. G. Chopra, M. L. Cohen, A. Zettl, S. G. Louie and V. H. Crespi, *Chem. Phys. Lett*., 1998, 286, 490-496.

52. L. A. Girifalco and R. J. Good, *J. Phys. Chem.*, 1957, 61, 904-909.

53. M. Hodak and L. A. Girifalco, *Chem. Phys. Lett*., 2001, 350, 405-411.

54. R. Zacharia, H. Ulbricht and T. Hertel, *Phys. Rev. B*, 2004, 69, 155406.

55. J.-S. Yeo, J.-M. Yun, M. Kang, D. Kim, S.-H. Lee, S.-S. Kim, S.-I. Na and D.-Y. Kim, *ACS Appl. Mater. Interfaces*, 2014, 6, 19613−19620.

56. J. P. Thomas, L. Zhao, D. McGillivray and K. T. Leung, *J. Mater. Chem. A*, 2014, 2, 2383–2389.

57. Y. H. Kim, C. Sachse, M. L. Machala and C. May, *Adv. Funct. Mater*., 2011, 21, 1076–

1081.

58. J.-G. Chen, H.-Y. Wei and K.-C. Ho, *Sol. Energy Mater. Sol. Cells*, 2007, 91, 1472–1477.

59. B, Zhang, G. Tan, C.-S. Lam, B. Yao, C.-L. Ho, L. Liu, Z. Xie, W.-Y. Wong, J. Ding and L. Wang, L. *Adv. Mater*., 2012, 24, 1873–1877.

60. Z.-T. Zhu, J.T. Mabeck, C. Zhu, N. C. Cady, C. A. Batt and G. G. Malliaras, *Chem. Commun*., 2004, 1556-1557.

61. M. Kus and S. Okur, *Sens. Act. B*, 2009, 143, 177–181.

62. B. Gupta, M. Mehta, A. Melvin, R. Kamalakannan, S. Dash, M. Kamruddin and A.K. Tyagi, *Materials Chemistry and Physics*, 2009, 147, 867-877.

63. X. Wu, J. Liu, D. Wu, Y. Zhao, X. Shi, J. Wang, S. Huang and G. He, *J. Mater. Chem. C*, 2014, 2, 4044-4050.

64. H. Park, Y. Shi and J. Kong, *Nanoscale*, 2013, 5, 8934-8939.

65. D. Alemu, H. –Y. Wei, K. –C. Ho and C. –W. Chu, *Energy Environ. Sci.*, 2012, 5, 9662-9671.

66. J. Seo, S. Park, Y. C. Kim, N. J. Jeon, J. H. Noh, S. C. Yoon and S. I. Seok, *Energy Environ. Sci.*, 2014, **7,** 2642-2646.

67. T. –W. Lee and Y. Chung, *Adv. Funct. Mater.,* 2008, 18, 2246-2252.

68. D. Eichinger, C. Lotz and A. G. Lenring, *Lenzinger Berichte*, 1996, 75, 69-72.

69. R. L. D. Whitby, A. Korobeinyk, V. M. Gun'ko, R. Busquets, A. B. Cundy, K. László, J. Skubiszewska-Zieba¸ R. Leboda, E. Tombacz, I. Y. Toth, K. Kovacs and S. V. Mikhalovsky, *Chem. Commun*., 2011, 47, 9645-9647.

70. C. Chen, W. Kong, H. –M. Duan and Jun Zhang, *Phys. Chem. Chem. Phys.*, 2014, 16, 12858-12864.

71. N. B. Godfrey, *Chemtech*, 1972, 6, 359-363.

72. Y. Si and E. T. Samulski, *Nano Lett.*, 2008, 8, 1679-1682.

73. U. Khan, A. O'Neill, M. Lotya, S. De and J. N. Coleman, *Small*, 2010, 6 864-871.

74. P. May, U. Khan, J. M. Hughes and J. N. Coleman, *J. Phys. Chem. C*, 2012, 116, 11393-11400.

75. U. Khan, H. Porwal, A. O'Neill, K. Nawaz, P. May and J. N. Coleman, *Langmuir*, 2011, 27, 9077-9082.

76. M. Yi, Z. Shen, X. Zhang and S. Ma, *J. Phys. D: Appl. Phys.*, 2013, 46, 025301.

77. U. Khan, A. O'Neill, H. Porwal, P. May, K. Nawaz and J. N. Coleman, *Carbon*, 2012, 50, 470-475.

78. Y. Wen, K. He, Y. Zhu, F. Han, Y. Xu, I. Matsuda, Y. Ishii, J. Cumings and C. Wang, *Nature Communications*, 2014, 5, 4033.

79. G. Eda, G. Fanchini, and M. Chhowalla, *Nature Nanotech.,* 2008, 3, 270-274.

80. D. Yoon, H. Moon and H. Cheong, *J. Korean Phys. Soc.*, 2009, 55, 1299-1303.

81. H. C. Schniepp, J. –L. Li, M. J. McAllister, H. Sai, M. Herrera-Alonso, D. H. Adamson, R. K. Prud'homme, R. Car, D. A. Saville and I. A. Aksay, *J. Phys. Chem. B*, 2006, 110, 8535-8539.

82. G. H. Kim, D. H. Hwang and S. I. Woo, *Phys. Chem. Chem. Phys.*, 2012, 14, 3530-3536.

83. J. Franklin and Z. Y. Wang, *Chem. Mater.*, 2002, 14, 4487-4489.

84. D. –H. Kim and S. –Y. Park, *Polymer*, 2014, 55, 2928-2935.

Supplementary information

Figure SI 1. Solidified graphene mixture with $NMMO_m$ at room temperature after one month later.

(a) (b)

Figure SI 2. Photographs of the GPN dispersion in water at C_{GPN} = 1 mg/mL: (a) immediately and (b) 3 months after sonication for 2 h; the laser beams in the vials are to used to observe the Tyndall effect.

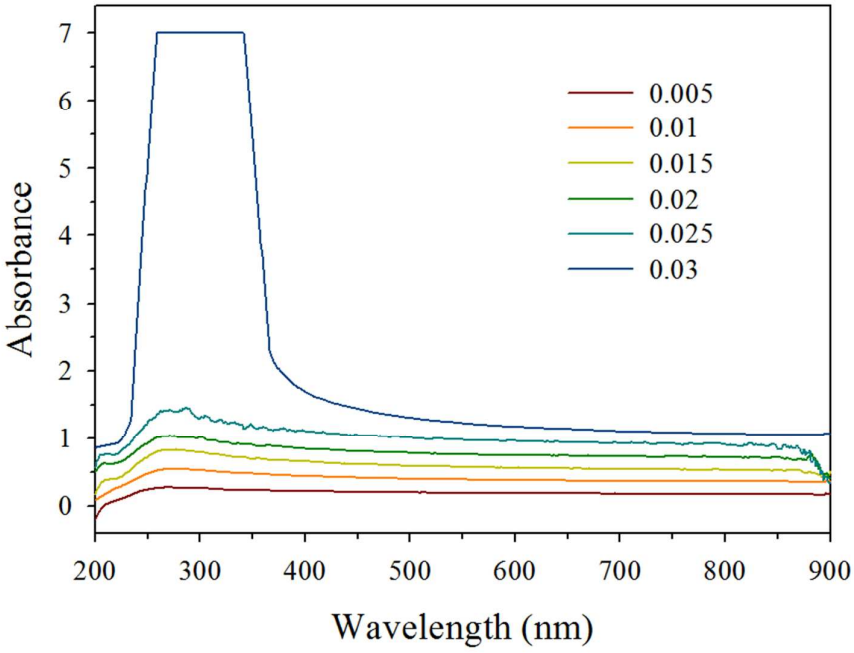

Figure SI 3. UV-Vis spectra with different C_{GPN}s in the range of 0.005 to 0.03 mg/mL.

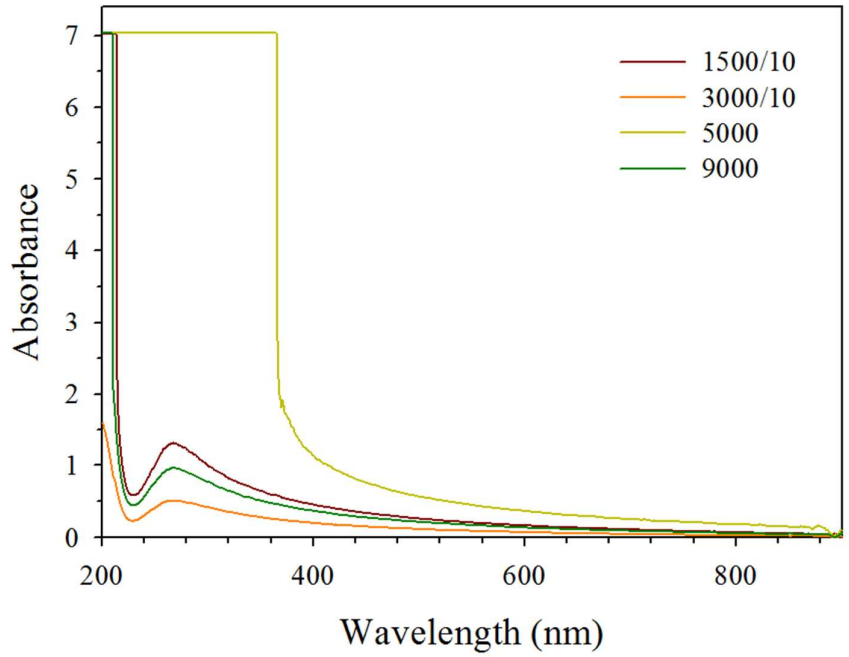

Figure SI 4. UV-Vis spectra after centrifugation of the 5 mg/mL GPN solution at 1,500, 3,000, 5,000, and 9,000 rpm; the absorbance at 1,500 and 3,000 rpm were obtained from × 10 dilution with water after centrifugation.

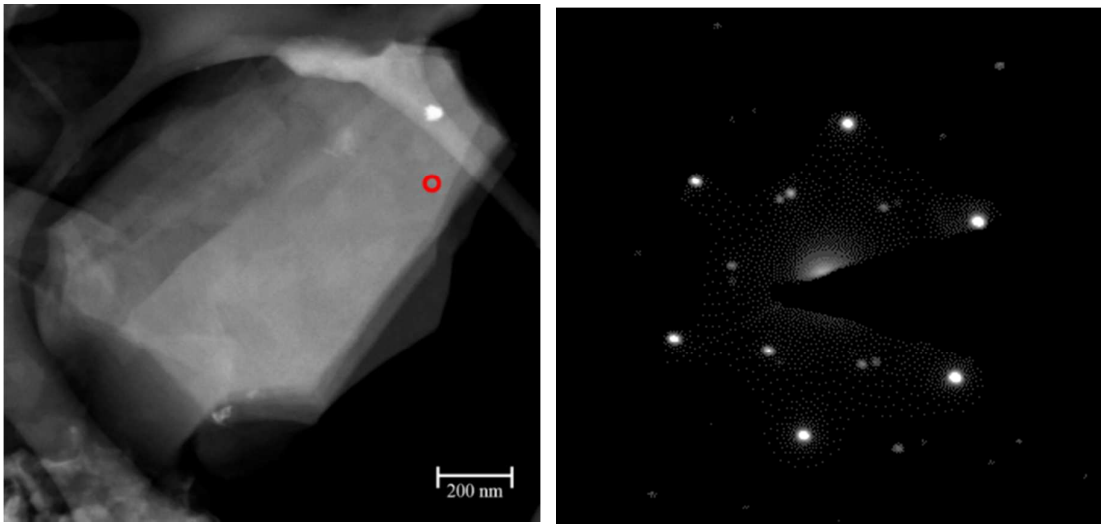

(a) (b)

Figure SI 5. (a) STEM image and (b) SAED pattern of the multi-layered graphene in the circled area in (a).